Supporting Information

Boosting electrocatalytic nitrate-to-ammonia conversion via plasma enhanced CuCo alloy-substrate interaction

Angjian Wu[a*#], Yimeng Zhou[a#], Jiabao Lv[a], Delong Zhang[b], Yaqi Peng[a], Qiulin Ye[a], Pengcheng Fu[b], Weitao Wang[c], Xiaoqing Lin[a], Shaojun Liu[a], Mengxia Xu[a,f], Zhifu Qi[d], Songqiang Zhu[d], Wei Zhu[e], Jianhua Yan[a], Xin Tu[c]*, Xiaodong Li[a]*

[a] State Key Laboratory of Clean Energy Utilization, Zhejiang University, Hangzhou, 310027, P. R. China

[b] Interdisciplinary Center for Quantum Information, Zhejiang Province Key Laboratory of Quantum Technology and Device, and Department of Physics, Zhejiang University, Hangzhou, P. R. China

[c] Department of Electrical Engineering and Electronics, University of Liverpool, Liverpool L69 3GJ, United Kingdom

[d] Zhejiang Energy Technology Research Institute Co. Ltd., Hangzhou, 311121, P. R. China

[e]State Key Lab of Organic-Inorganic Composites, Beijing University of Chemical Technology, Beijing 100029, China.

[f]Department of Chemical and Environmental Engineering, University of Nottingham Ningbo China, Ningbo 315100, China

*Corresponding authors.

Email addresses: wuaj@zju.edu.cn (A. Wu),

xin.tu@liverpool.ac.uk (X. Tu),

lixd@zju.edu.cn (X. Li)

[#] These authors contributed equally to this work.

Number of pages: 11

Number of figures: 14

Number of tables: 2

Supplementary figures and tables.

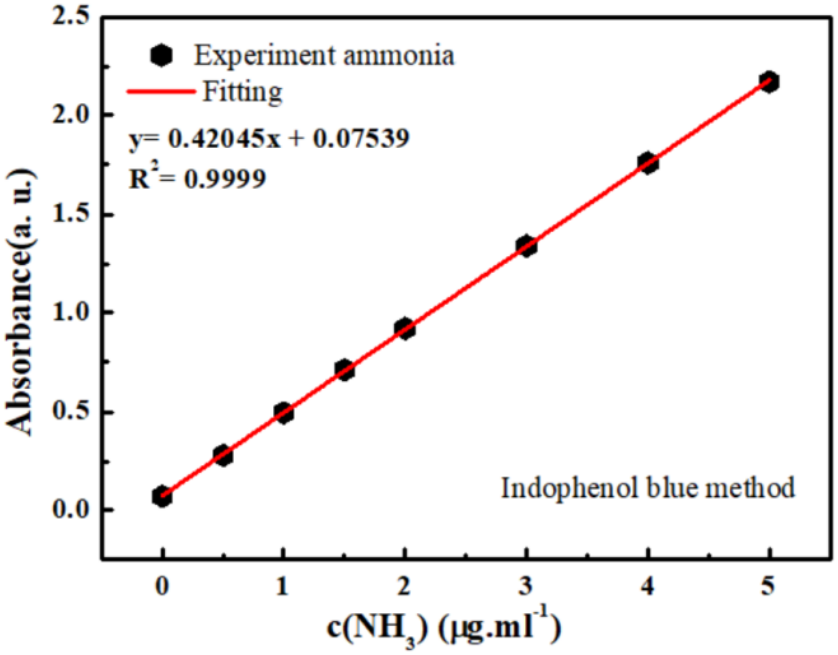

Figure S1. The standard solution for quantitatively measuring NH_3 concentration.

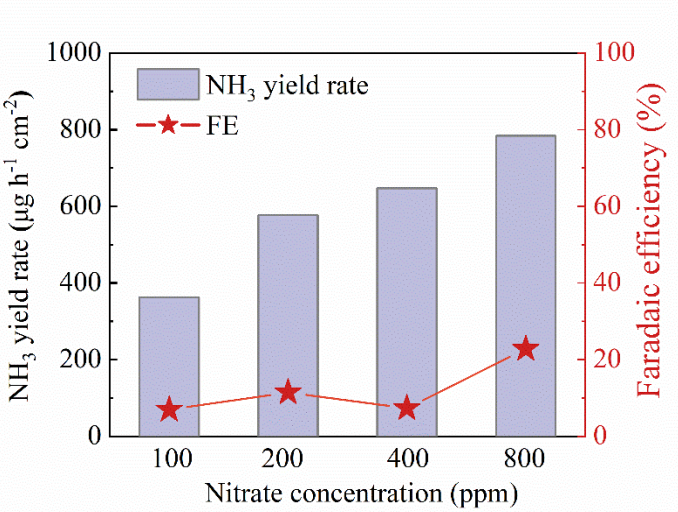

Figure S2. The NH_3 yield rate and FE at -0.67 V vs. RHE using the $Cu_{80}Co_{20}$ catalyst at low nitrate concentration (100 to 800 ppm).

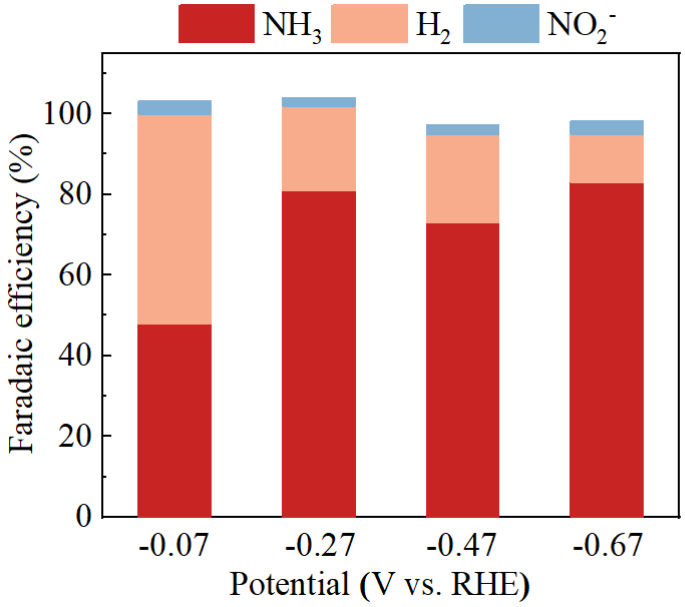

Figure S3. Measurement of all products using the $Cu_{80}Co_{20}$ catalyst at a potential range from -0.07 V to -0.67 V vs. RHE.

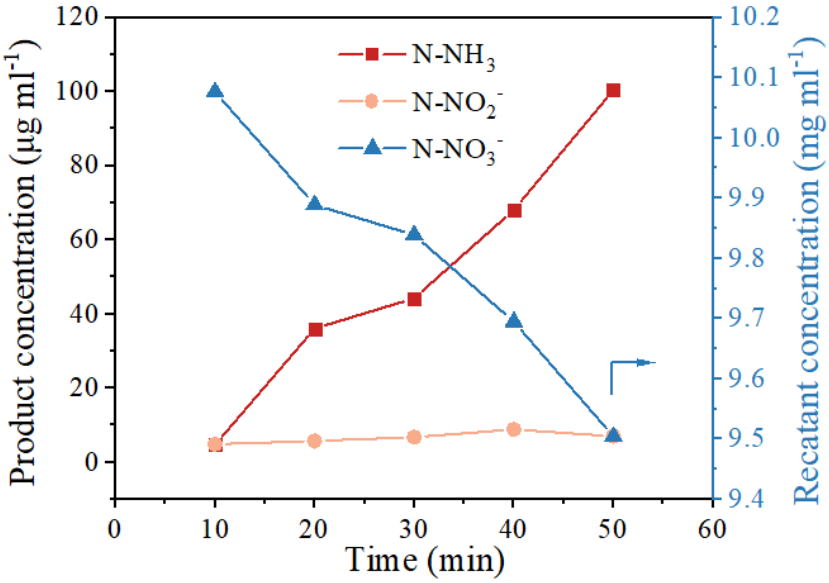

Figure S4. Changes in the concentration of nitrogen species (NO_3^- , NO_2^-, and NH_3) during electrocatalysis on $Cu_{80}Co_{20}$ in 1 h (-0.67 V vs. RHE).

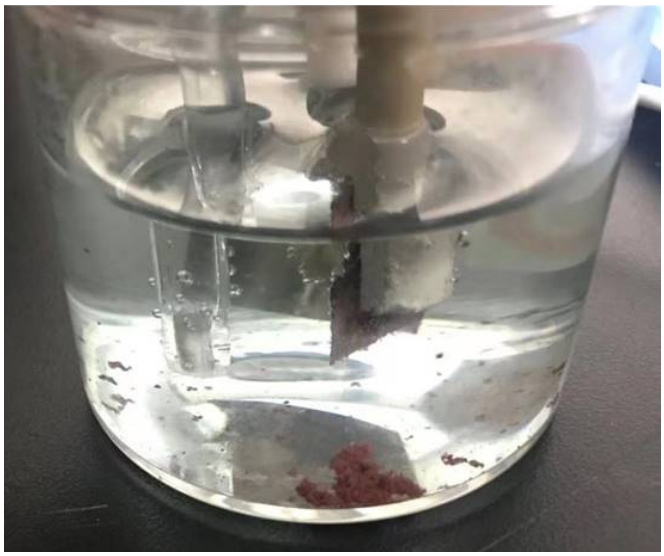

Figure S5. CuCo catalyst electrodeposition process without plasma pre-treatment.

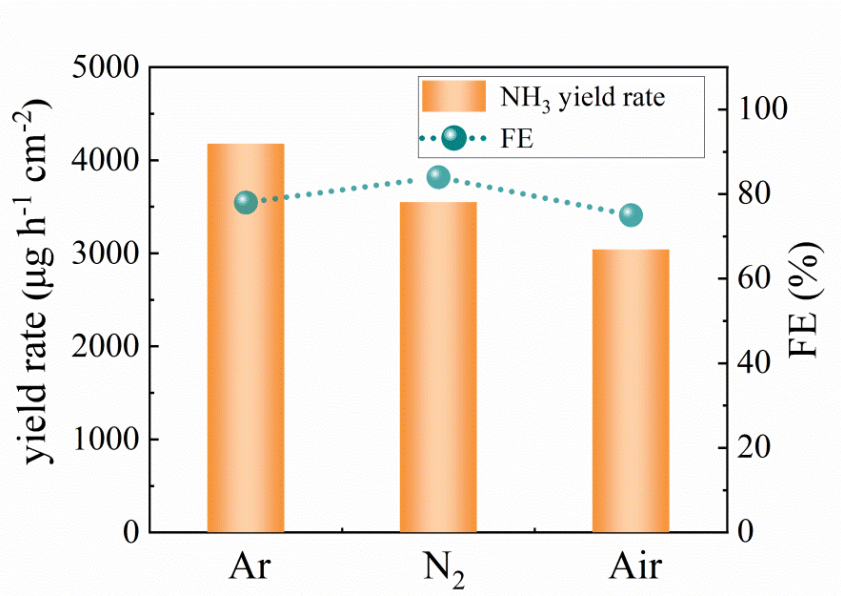

Figure S6. The NH_3 yield rate and FE using plasma modified CuCo alloy with different working gases (Ar, N_2 and Air).

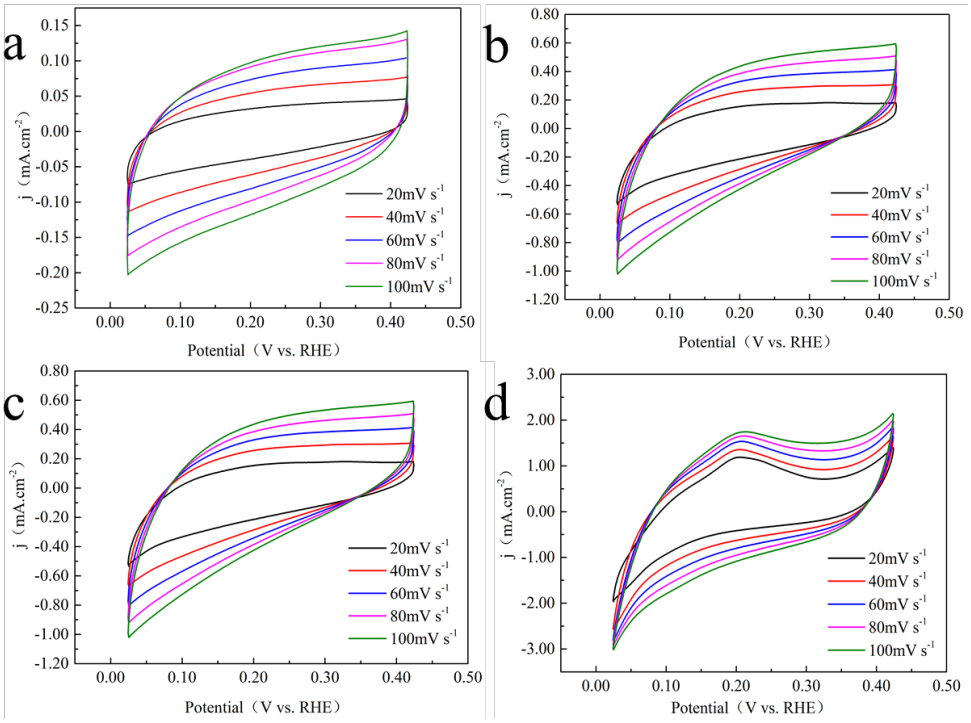

Figure S7. Cyclic voltammogram curves of the untreated pure Cu (a), $Cu_{30}Co_{70}$ (c), and Ar-plasma modified pure Cu (b), $Cu_{30}Co_{70}$ (d) catalyst. The cyclic voltammetry profiles were obtained using the pure Cu and $Cu_{30}Co_{70}$ catalysts at the sweep rates of 20, 40, 60, 80, and 100 mV s^{-1}.

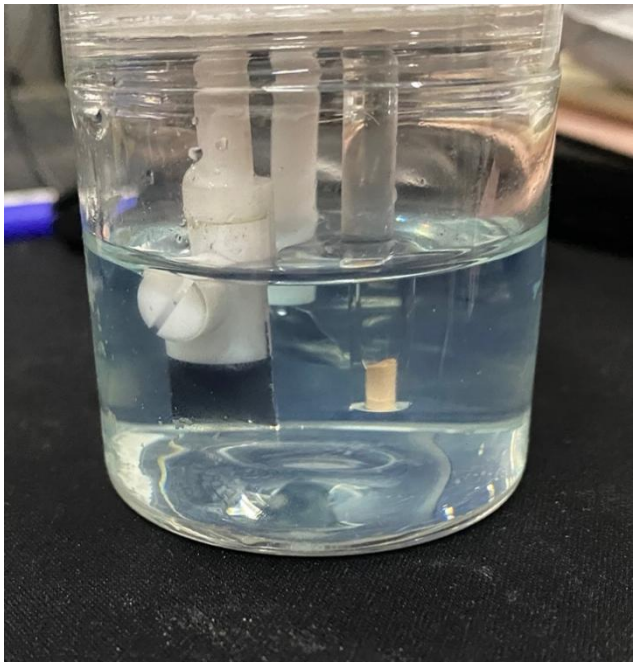

Figure S8. CuCo catalyst electrodeposition process after ICP Ar-plasma treatment with power and treatment duration of 300 w and 5 mins, respectively.

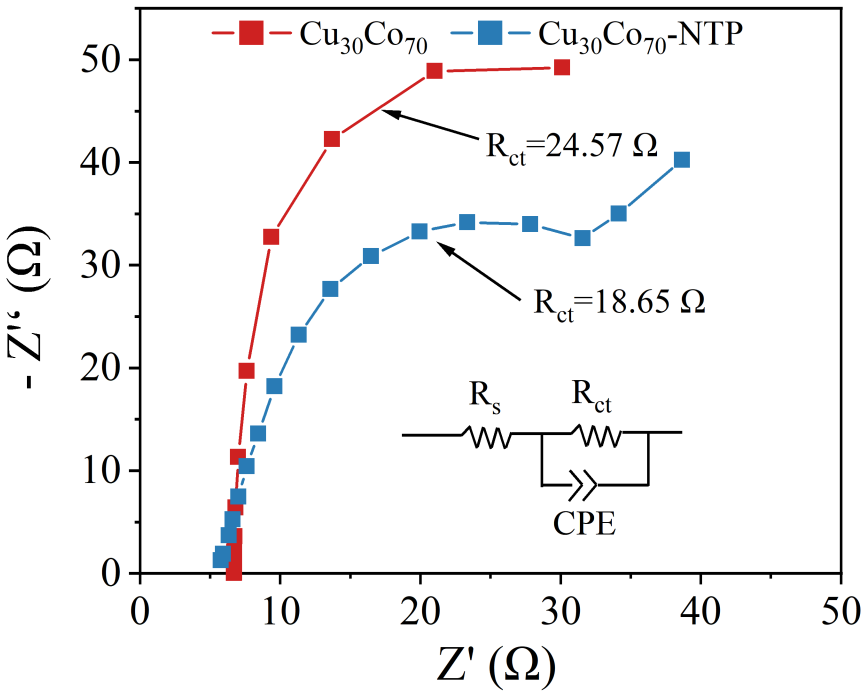

Figure S9. EIS spectra from 0.01 Hz to 10000Hz at open circuit potential of $Cu_{30}Co_{70}$ and $Cu_{30}Co_{70}$-NTP.

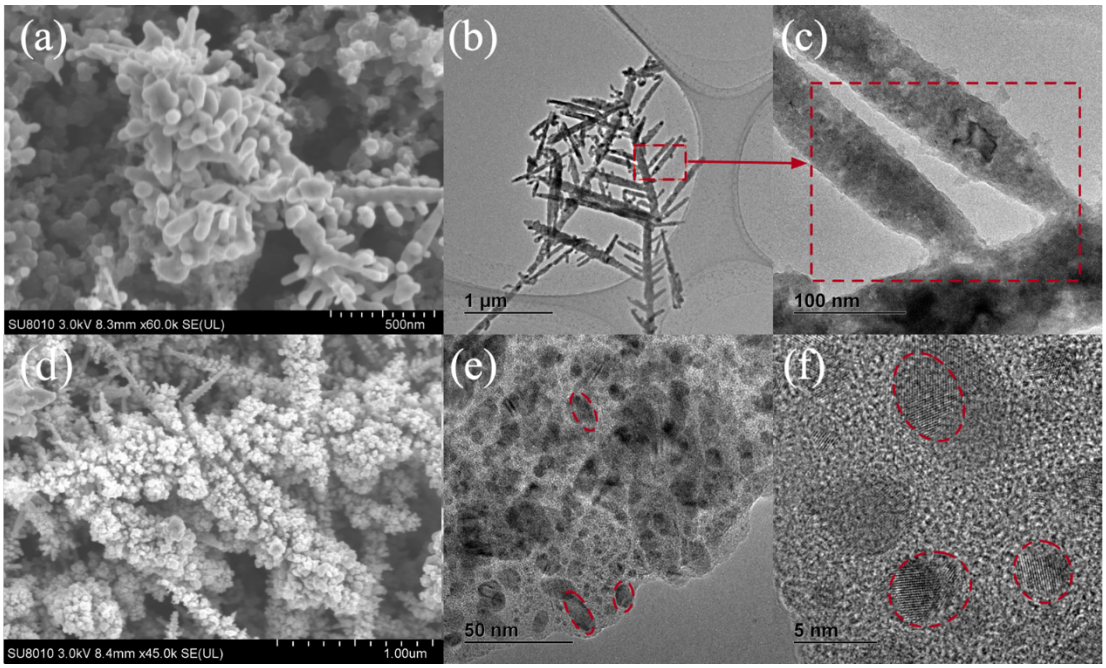

Figure S10. TEM images of the pure Cu (a-c) and $Cu_{30}Co_{70}$ (d-f) catalysts deposited on substrate with Ar-plasma treatment.

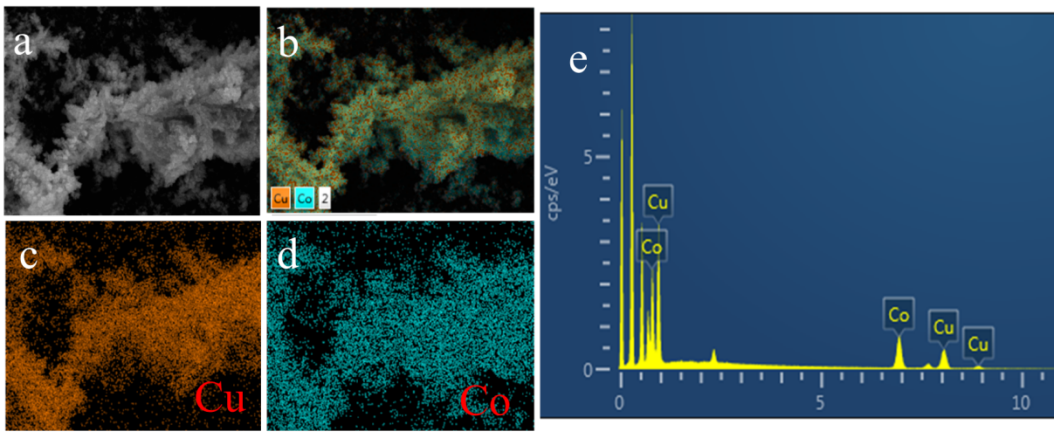

Figure S11 Energy Dispersive Spectrometer (EDS) images of the $Cu_{30}Co_{70}$ catalyst with Ar-plasma treatment in the selected region. The scale bars are 5 μm. The weight ratio of Co was about 35%, and the weight ratio of Cu was about 65%. (a) Catalyst morphology. (b) Cu and Co in EDS spectra. (c) Cu in EDS spectra. (d) Co in EDS spectra. (e) Elements composition.

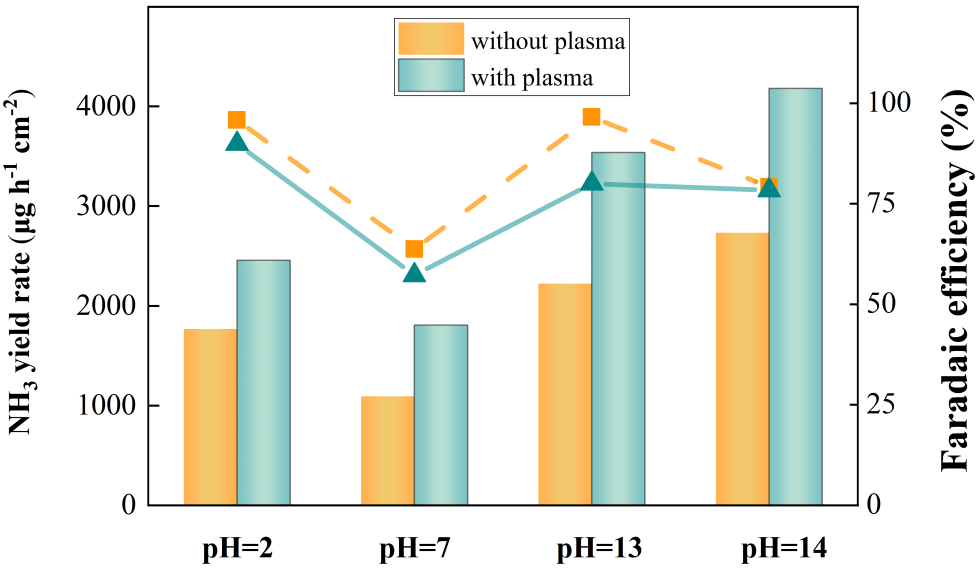

Figure S12. Comparison of nitrate-to-NH_3 activity using CuCo alloy before and after Ar-plasma treatment in terms of pH variation at -0.27 V vs. RHE.

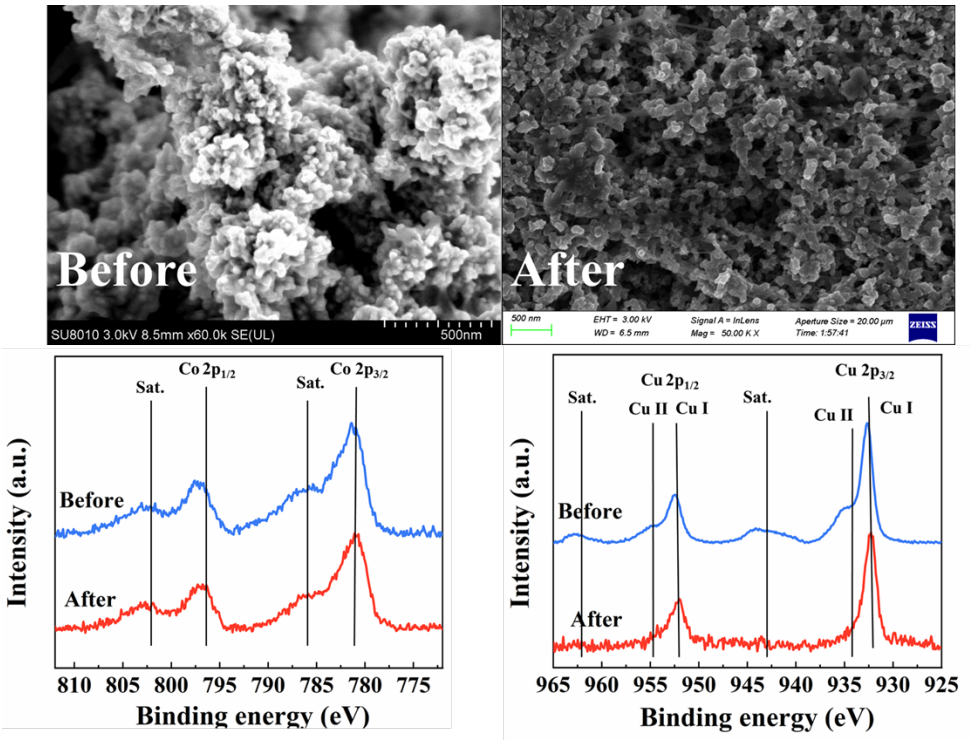

Figure S13. SEM and XPS iamges of the long-term working and non-working $Cu_{30}Co_{70}$ catalyst.

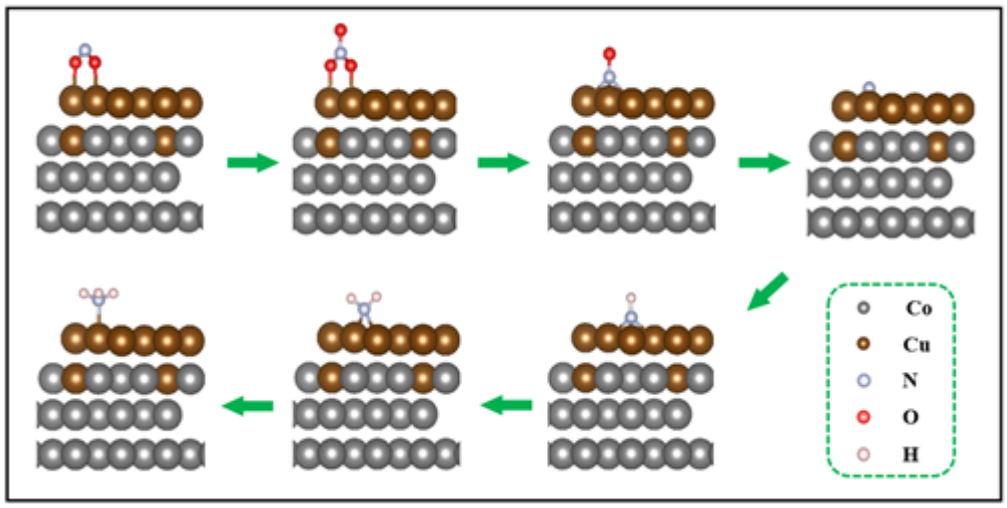

Figure S14. Stable structure and intermediate pathways for the reduction of ammonia by CuCo catalysts.

Table S1 Actual loading amount of Cu and Co on different catalysts obtained by ICP-OES

	Cu (μg cm^{-2})	Co (μg cm^{-2})
Cu	41.23	0.321
Co	0.772	45.77
$Cu_{30}Co_{70}$	9.33	39.75
$Cu_{50}Co_{50}$	22.52	28.34
$Cu_{80}Co_{20}$	50.11	12.33

Table S2 Comparison of different electrocatalysts for NH_3 synthesis from nitrate.

Cathode material	FE_{max}	j_{NH3} (mA cm^{-2})	Production rate (μg h^{-1} cm^{-2})	Production rate (mmol mg_{cat}^{-1} h^{-1})	Ref.
Titanium	82%	22	/	/	[1]
Copper-molecular solid	85.9%	40	436	/	[2]
Copper nanosheets	99.7%	12	400	/	[3]
Copper-nickel Alloys	98%	160	/	/	[4]
TiO_{2-x}	85%	/	/	0.045	[5]
Cu/Cu_2O NWAs	95.8%	/	3330.6	/	[6]
Iron-based single-atom	~100%	/	2750 .7	/	[7]
Strained ruthenium nanoclusters	~100%	> 120	/	5.56	[8]
CuCo alloy modified by Ar-plasma	**78.4% ~92.2 %**	**90**	**4180.7**	**/**	**This work**

Supplementary notes 1

Characterization of Super-resolution infrared imaging

Super-resolution infrared imaging was performed by a mid-infrared photothermal (MIP) imaging and spectroscopy platform (mIRage, Photothermal Spectroscopy Corp.), which is comprised of a mid-infrared 100 kHz pulsed pump laser and a 532-nm continuous-wave (CW) laser as the probe beam, collinearly focused by a reflective objective (40X, 0.78 N.A.) onto the sample. The IR absorption induces a photothermal signal that modulates the probe intensity, which was epi-detected at a photodiode. The modulation signal was then extracted by a phase-sensitive detection with a lock-in amplifier (MFLI, Zurich Instruments). MIP spectra were acquired ranging from 1215 to 1800 cm^{-1} and 1980 to 2321cm^{-1} with 20 ms time constant, 2 cm^{-1} step density and 100 cm^{-1}/s tuning speed. Each spectrum was averaged for 4 times. All MIP imaging were acquired with a 500-nm spatial step size and a 1.04-Hz scan rate. IR and CW probe power were set at 45% and 11%, respectively, for all spectra and images.

Supplementary notes 2

A Nicolet iS50 FT-IR transform infrared spectrometer equipped with a mercury cadmium telluride detector cooled with liquid nitrogen was employed in the IRRAS study. A calcium fluoride window and an in-situ EC-IR thin cell were applied in the test. The angle of incidence was set as ca. 70°. The working electrode was a glassy carbon electrode (6 mm in diameter) with drop-casted catalysts. The Ag/AgCl and Pt wire were used as reference electrode and counter electrode, respectively. The surface of working electrode was pressed onto the calcium fluoride window with a gap less than 10 m when collecting IR spectrum. The electrolyte was 1 M KOH and 0.1 M KNO_3. In this experiment, chronopotentiometry was used at different potentials (-0.9 ~ -1.2 V vs. Ag/AgCl) after activation of catalyst. The reference spectrum was collected at -0.8 V. The spectra are given in absorption units defined as $A = -\log(R/R0)$, where R and R0 represent the reflected IR intensities corresponding to the sample- and reference-single beam spectrum, respectively.

Supplementary notes 3

NH_3 quantification via the indophenol blue method

The quantification of generated NH_3 was spectrophotometrically determined by the indophenol blue method. 1 mL of the reacted solution was extracted from the cathode half-cell vessel and then diluted to 4 mL for detection. Afterward, 0.32 mL of 1 wt% sodium nitroferricyanide aqueous solution was added into diluted samples, followed by the addition of 2.4 mL of 0.32 M NaOH solution containing 10.4 M Sodium salicylate, and 0.8 mL of 0.3 M NaClO and 0.75M NaOH mixture. After 2 hours of incubation, the sample was measured using a UV-vis spectrophotometer. The concentration of

indophenol blue was determined according to the absorbance at the wavelength of 655 nm.

References

1. McEnaney, J. M.; Blair, S. J.; Nielander, A. C.; Schwalbe, J. A.; Koshy, D. M.; Cargnello, M.; Jaramillo, T. F. Electrolyte Engineering for Efficient Electrochemical Nitrate Reduction to Ammonia on a Titanium Electrode. *ACS Sustain. Chem. Eng*. **2020**, 7, 2672-2681, DOI 10.1021/acssuschemeng.9b05983.
2. Dima, G. E.; Vooys, A. C. A.; Koper, M. T. M. Electrocatalytic reduction of nitrate at low concentration on coinage and transition-metal electrodes in acid solutions, *J. Electroanal. Chem.* **2003**, 554, 15-23, DOI 10.1016/S0022-0728(02)01443-2.
3. Fu, X.; Zhao, X.; Hu, X.; He, K.; Yu, Y.; Li, T.; Tu, Q.; Qian, X.; Yue, Q.; Wasielewski, M. R.; Kang, Y. Alternative route for electrochemical ammonia synthesis by reduction of nitrate on copper nanosheets. *Appl. Mater*, **2020**, 4, 100620, DOI 10.1016/j.apmt.2020.100620.
4. Wang, Y.; Xu, A.; Wang, Z.; Huang, L.; Li, J.; Li, F.; Wicks, J.; Luo, M.; Nam, D.; Tan, C.; Ding, Y.; Wu, J.; Lum, Y.; Dinh, C.; Sinton, D.; Zheng, G.; Sargent, E. H. Enhanced Nitrate-to-Ammonia Activity on Copper-Nickel Alloys via Tuning of Intermediate Adsorption. *J. Am. Chem. Soc*. **2020**, 142, 5702-5708, DOI 10.1021/jacs.9b13347.
5. Jia, R.; Wang, Y.; Wang, C.; Ling, Y.; Yu, Y.; Zhang, B. Boosting Selective Nitrate Electroreduction to Ammonium by Constructing Oxygen Vacancies in TiO_2. *ACS Catal*, **2020**, 10, 3533-3540, DOI 10.1021/acscatal.9b05260 .
6. Wang, Y.; Zhou, W.; Jia, R.; Yu, Y.; Zhang, B. Unveiling the Activity Origin of a Copper-based Electrocatalyst for Selective Nitrate Reduction to Ammonia. *Angew. Chem. Int. Ed.* **2020**, 59, 5350-5354, DOI 10.1002/anie.201915992.
7. Li, P.; Jin, Z.; Fang, Z.; Yu, G. A single-site iron catalyst with preoccupied active center that achieves selective ammonia electrosynthesis from nitrate. *Energy Environ. Sci*. **2021**, 14, 3522-3531, DOI 10.1039/D1EE00545F.
8. Li, J.; Zhan, G.; Yang, J.; Quan, F.; Mao, C.; Liu, Y.; Wang, B.; Lei, F.; Li, L.; Chan, A. W. M.; Xu, L.; Shi, Y.; Du, Y.; Hao, W.; Wong, P. K.; Wang, J.; Dou, S.; Zhang, L.; Yu, J. C. Efficient Ammonia Electrosynthesis from Nitrate on Strained Ruthenium Nanoclusters. *J. Am. Chem. Soc*. **2020**, 142, 7036-7046, DOI 10.1021/jacs.0c00418.